© 2019. Published by The Company of Biologists Ltd | Journal of Cell Science (2019) 132, jcs232579. doi:10.1242/jcs.232579

RESEARCH ARTICLE

An acute decrease in plasma membrane tension induces macropinocytosis via PLD2 activation

Julie Loh[1,*], Mei-Chun Chuang[1,*], Shan-Shan Lin[1,*], Jophin Joseph[2], You-An Su[1], Tsung-Lin Hsieh[1], Yu-Chen Chang[1], Allen P. Liu[2] and Ya-Wen Liu[1,3,‡]

ABSTRACT

Internalization of macromolecules and membrane into cells through endocytosis is critical for cellular growth, signaling and plasma membrane (PM) tension homeostasis. Although endocytosis is responsive to both biochemical and physical stimuli, how physical cues modulate endocytic pathways is less understood. Contrary to the accumulating discoveries on the effects of increased PM tension on endocytosis, less is known about how a decrease of PM tension impacts on membrane trafficking. Here, we reveal that an acute decrease of PM tension results in phosphatidic acid (PA) production, F-actin and phosphatidylinositol (4,5)-bisphosphate [PI(4,5)P_2]-enriched dorsal membrane ruffling and subsequent macropinocytosis in myoblasts. The PA production induced by decreased PM tension depends on phospholipase D2 (PLD2) activation via PLD2 nanodomain disintegration. Furthermore, the 'decreased PM tension–PLD2–macropinocytosis' pathway is prominent in myotubes, reflecting a potential mechanism of PM tension homeostasis upon intensive muscle stretching and relaxation. Together, we identify a new mechanotransduction pathway that converts an acute decrease in PM tension into PA production and then initiates macropinocytosis via actin and PI(4,5)P_2-mediated processes.

KEY WORDS: PLD2 nanodomain, Phosphatidic acid, Mechanical transduction, Endocytosis

INTRODUCTION

Eukaryotic cells harness multiple endocytic pathways to internalize fluid and membrane into transport vesicles from the plasma membrane (PM) (Conner and Schmid, 2003; Doherty and McMahon, 2009). In response to various cellular demands and environmental stimuli, endocytic machineries are biochemically and physically regulated to govern the growth and survival of cells (Dai and Sheetz, 1995; Liu et al., 2017; Scita and Di Fiore, 2010). Among them, macropinocytosis is an endocytic pathway induced by biochemical stimuli, including nutrients, growth factors, integrin substrates or even viruses, which involves actin-based membrane ruffling and engulfment that leads to the formation of macropinosomes (Buckley and King, 2017; Doherty and McMahon, 2009).

Upon hyper-stimulation of growth factor receptors, activated phosphoinositide 3-kinase (PI3K) and small GTPases initiate macropinocytosis via phosphatidylinositol (3,4,5)-trisphosphate (PIP_3) production and actin polymerization (Levin et al., 2015; Yoshida et al., 2018). After membrane ruffling and closure, a sealed and large endocytic vacuole (1–10 µm in diameter) is formed. With the relatively large amount of solutes and membrane being internalized, macropinocytosis is an efficient route to quickly uptake nutrients (Bloomfield and Kay, 2016; Doherty and McMahon, 2009). In contrast to the understanding of the mechanism of biochemically induced macropinocytosis, little is known about the effects of mechanical alteration on macropinosome formation.

PM tension, the force exerted on PM, has emerged as a master integrator that governs distinct cellular processes, including membrane trafficking, cell migration, immunological responses, cell growth and differentiation (Dai and Sheetz, 1995; Diz-Muñoz et al., 2013; Masters et al., 2013). For endocytosis, cells need to overcome a higher energetic barrier to bend the membrane inwardly when PM tension is high, for example, by using the pulling force from actin polymerization in clathrin-mediated endocytosis (Boulant et al., 2011; Tan et al., 2015; Weinberg and Drubin, 2012). Conversely, when PM tension is decreased, it is easier for endocytic machinery to deform the membrane and, thus, facilitates endocytosis (Saleem et al., 2015; Shi and Baumgart, 2015).

Membrane–cytoskeleton adhesion and osmotic pressure contribute to PM tension (Gauthier et al., 2012). Although PM tension is used to control multiple cellular events, cells also need to maintain homeostasis of PM tension by sensing the change of tension and modulating their membrane area or cytoskeletal attachment via endocytosis, exocytosis, membrane invagination, actin polymerization or depolymerization (Diz-Muñoz et al., 2013; Gauthier et al., 2012; Nassoy and Lamaze, 2012). Together, a feedback regulation of PM tension, actin polymerization and membrane trafficking underpins PM tension homeostasis and membrane remodeling events in cells.

The sensors of PM tension are generally transmembrane proteins or peripheral membrane proteins, including stretch-activated ion channels, the caveolin–cavin complex, curvature-sensing proteins or membrane-actin-interacting proteins (Diz-Muñoz et al., 2013; Tsujita et al., 2015). Recently, Petersen et al. reported that the lipid raft could function as a mechanosensor that undergoes kinetic or mechanical disruption to activate phospholipase D2 (PLD2) (Petersen et al., 2016). PLD2 is a PM-localized lipase that catalyzes the conversion of phosphatidylcholine (PC) into phosphatidic acid (PA) and choline, and is involved in endocytosis and actin polymerization (Antonescu et al., 2010; Colley et al., 1997; Du et al., 2004; Jiang et al., 2016). PLD2 mainly localizes at lipid nanodomains, the lipid rafts, on PM via palmitoylation on its C223 and C224 residues, where

[1]Institute of Molecular Medicine, College of Medicine, National Taiwan University, Taipei 10002, Taiwan. [2]Department of Mechanical Engineering, University of Michigan, Ann Arbor, MI 48109, USA. [3]Center of Precision Medicine, College of Medicine, National Taiwan University, Taipei 10002, Taiwan.
*These authors contributed equally to this work

‡Author for correspondence (yawenliu@ntu.edu.tw)

A.P.L., 0000-0002-0309-7018; Y.-W.L., 0000-0003-0180-4142

Received 1 April 2019; Accepted 29 July 2019

Journal of Cell Science (2019) 132, jcs232579. doi:10.1242/jcs.232579

PC and phosphatidylinositol (4,5)-bisphosphate [$PI(4,5)P_2$], its substrate and activator, are excluded (Xie et al., 2002). Chemical or mechanical disruption of lipid raft may release the segregated PLD2 and thus enhance PA production at the PM (Diz-Muñoz et al., 2016; Petersen et al., 2016).

PA is a negatively charged, cone-shaped lipid identified as a key mediator in phospholipid metabolism, mammalian target of rapamycin (mTOR) activation, membrane trafficking, mitochondrial fusion and actin polymerization (Liu et al., 2013; Yang and Frohman, 2012). PA could be produced through phospholipid synthesis (the Kennedy pathway) in the endoplasmic reticulum, the phosphorylation of diacylglycerol by diacylglycerol kinase, or the hydrolysis of PC by PLD on plasma or endosomal membranes (Liu et al., 2013). Given that the activity of PLD2 is regulated by mechanical cues, as well as the importance of its enzymatic product, PA, on actin polymerization and membrane trafficking, we hypothesize that alteration of PM tension may affect PLD2 activity thus affects endocytosis. Here, we discover that an acute decrease of PM tension induces PA production, which triggers macropinocytosis without eliciting an increase in PIP_3.

RESULTS

PA is enriched at dorsal membrane ruffles upon the decrease of PM tension

To examine the direct effect of PM tension on PLD activity, we utilized hypotonic or hypertonic buffer to induce the increase or decrease of PM tension, respectively, in mouse myoblasts, similar to the approach taken by numerous prior studies (Boulant et al., 2011; Diz-Muñoz et al., 2013; Houk et al., 2012). After transfection of a PA biosensor (PABD–GFP, the PA-binding domain of yeast Spo20p fused with GFP) into C2C12 myoblasts, we imaged its distribution with spinning disc confocal microscopy at 37°C. Similar to a previous report (Zeniou-Meyer et al., 2007), PABD–GFP was mainly distributed in the nucleus and PM, especially at lamellipodia and membrane ruffles when cells were incubated in an isotonic buffer (1× PBS) (Fig. 1Aa). Interestingly, the enriched signals of PABD–GFP at PM became diffused after a 2-min incubation in a hypotonic buffer (0.5× PBS) (Fig. 1Ab), and they re-appeared when the cells were allowed to recover in 1× PBS for 2 min (Fig. 1Ac; Movie 1). We hereafter referred to this hypotonic treatment followed with isotonic buffer recovery as osmotic shock (OS) treatment.

A similar phenotype could be observed when directly incubating the cells with a hypertonic buffer (PBS+150 mM sucrose) where the PABD–GFP signal at membrane ruffles increased from 2 min, peaked at 5 min and gradually settled (Fig. 1B; Fig. S1A, Movie 2). We thus quantified the effect of hypertonic buffer treatment on membrane ruffling by dividing the ruffling phenotype into four categories: sparse, mild, intermediate and severe with <5%, 5–10%, 10–20% or >20% of the dorsal area having membrane ruffles, respectively (Fig. 1C). While only 5% of cells incubated in isotonic buffer had substantial membrane ruffles (intermediate and severe), a 5-min hypertonic buffer incubation significantly increased this population to 52%. Importantly, the PABD–GFP ruffles could also be observed when the decreased PM tension was induced with a radial cell stretcher by 2 min mechanical stretching and 2 min relaxation in myoblasts (Fig. 1D). Together, we found that PABD–GFP signal at PM was enhanced when PM tension was reduced by OS or mechanical stretch.

To test whether the enrichment of PABD–GFP at PM reflects a change of cellular PA level upon tension alteration, we extracted total lipids from cells treated with different buffers, measured the amount of PA with an enzymatic assay, normalized to the protein concentrations and expressed it as fold change compared with the control cells. Consistent with the data for PABD–GFP signals at the PM, the total PA amount in hypertonic buffer-treated cells was increased with a similar kinetics to the PABD–GFP signals, increasing gradually and peaking at 5 min (Fig. 1E; Fig. S1B). Surprisingly, both tension manipulations, hypertonic and hypotonic, led to increased total PA (Fig. 1E). These results suggest that total PA quantification may not reflect local PA production or distribution. To specifically investigate the effect of PM tension on PA dynamics, we thus mainly used PABD–GFP and live-cell imaging to further dissect this phenomenon.

Components of the dorsal membrane ruffles induced by decreased PM tension

To identify what the PA-rich membrane ruffles induced by a decrease in PM tension contain, we examined several PM components, including F-actin, dynamin-2 (Dyn2, also known as DNM2), $PI(4,5)P_2$ (labeled with PLC-PH–GFP), PIP_3 (labeled with Akt-PH–GFP), clathrin-coated pit adaptor protein (μ2–GFP; μ2 is also known as AP2M1) and caveolin-1 (Fig. 2A–D; Fig. S2A,B). In line with the function of PA on actin polymerization, we observed F-actin enrichment on the PABD–GFP ruffles where the membrane fission enzyme Dyn2 was also localized to (Fig. 2A,B). Owing to the observation that Lifeact–RFP expression slowed down membrane ruffle formation, we decided to use Dyn2–mCherry to mark the membrane ruffles induced by decreased PM tension for analysis between different pairs of markers. Interestingly, while $PI(4,5)P_2$ was enriched and colocalized with Dyn2–mCherry, neither PIP_3 nor μ2–GFP and caveolin-1–GFP were enriched at those membrane ruffles (Fig. 2C,D; Fig. S2A,B).

Interestingly, although exogenous caveolin-1–GFP and endogenous caveolin-1 were not enriched at the PA-rich membrane ruffles (Fig. S2B,C), the caveolin-1–GFP puncta appeared slightly increased or enlarged upon hypertonic treatment, potentially suggesting an increase in caveolae-dependent endocytosis (Fig. S2D).

To further visualize the membrane ruffles in three dimensions when a cell encounters the acute decrease in PM tension, we imaged the cell before and after hypertonic buffer treatment along the *z*-axis. After three-dimensional (3D) reconstruction, we found that PABD–GFP- and Dyn2–mCherry-enriched membrane ruffles were distributed at the peripheral dorsal membrane (open arrowheads in Fig. 2E). The decrease of cell volume upon hypertonic buffer incubation could be observed in the orthogonal image, where there was a reduction in cell height without changing cell width (Fig. 2F). Notably, most the PA and Dyn2-enriched membrane ruffles existed at the dorsal membrane. Together, we found that an acute decrease of PM tension results in F-actin- and PA-enriched membrane ruffle formation at the peripheral dorsal surface of the cell.

An acute decrease of PM tension induces macropinocytosis

The F-actin- and Dyn2-rich structures induced by decreased PM tension were reminiscent of the membrane ruffles during macropinocytosis. To examine whether micropinocytosis was occuring, we incubated PABD–GFP-expressing cells in buffers containing a macropinocytosis-specific cargo, 70 kDa Rhodamine-conjugated dextran (Rh-Dextran) (Wang et al., 2014). While little dextran signal was detected in cells incubated with isotonic buffer, several red puncta of ∼1 μm in diameter were observed at the cell periphery in hypertonic buffer- and OS-treated cells together with

Journal of Cell Science (2019) 132, jcs232579. doi:10.1242/jcs.232579

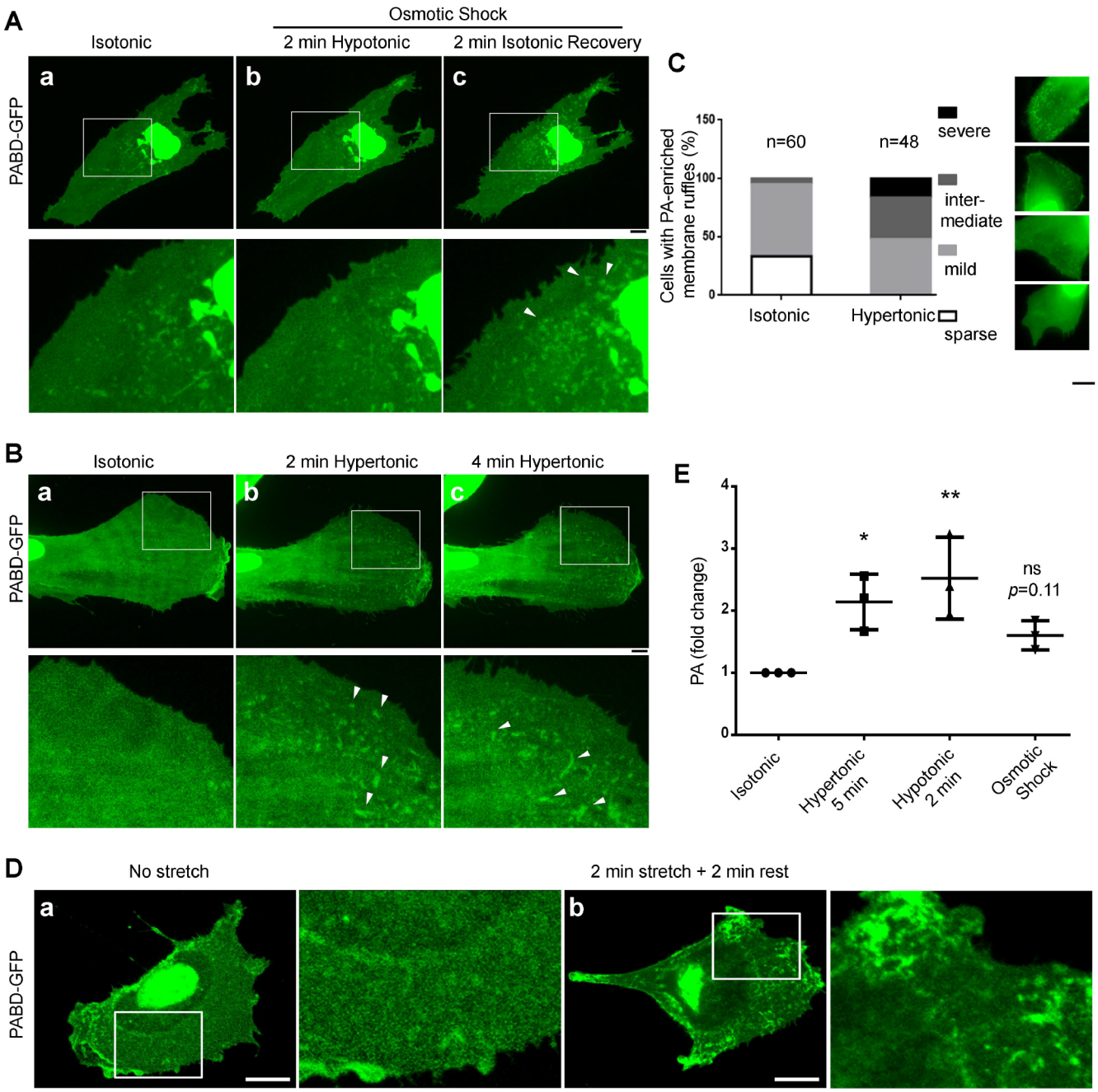

Fig. 1. Effects of PM tension manipulation on PA in myoblasts. (A) An increase of membrane tension suppresses PA-rich ruffles at PM. A PABD–GFP-expressing C2C12 myoblast was first imaged in isotonic buffer (Aa, 1× PBS), and two images were further captured after 2 min of hypotonic buffer (Ab, 0.5× PBS) and additional 2 min of 1× PBS recovery (Ac). Boxed areas are magnified and shown in the lower panel. (B) A decrease of tension induces PA enrichment at PM. A PABD–GFP-expressing myoblast was first imaged in isotonic buffer (Ba), and two images were further captured after 2 min (Bb) or 4 min (Bc) after hypertonic buffer treatment (1× PBS+150 mM sucrose). Arrowheads, PA-enriched membrane ruffles. (C) Quantification of membrane ruffling in cells treated with isotonic or for 5 min with hypertonic buffer. Ruffling phenotypes were divided into four categories with different levels or areas of membrane ruffle quantified by ZEN software. Three independent sets of experiments with a total of more than 48 cells were quantified for each condition. (D) PABD–GFP distribution upon mechanical stretch. PABD–GFP-expressing myoblasts were subjected to 0% (Da) or 20% radial stretch for 2 min (Db). After 2 min of relaxation, myoblasts were fixed and imaged with confocal microscopy. Boxed areas are magnified and shown on the right. (E) Effects of different osmotic buffers on cellular PA amount. Myoblasts treated with indicated buffers were harvested and extracted for total lipids. The total PA:protein ratio was compared with that from the isotonic buffer-treated cells. Results are mean±s.d. of at least three independent experiments. *P<0.05, **P<0.01; ns, not significant (one-way ANOVA followed by Dunnet's post-hoc test). Scale bars: 10 µm.

prominent PABD–GFP ruffles (Fig. 3A, arrowheads). After quantification, we found that OS- and hypertonic buffer-treated cells have a significantly enhanced fluorescence intensity of dextran compared with cells in isotonic buffer (Fig. 3B).

We further quantified the number of dextran puncta larger than 0.5 µm, the characteristic size of a macropinosome, and neglected smaller ones that could be caused by other endocytic pathways. The quantification results showed that both OS and hypertonic buffer

Journal of Cell Science (2019) 132, jcs232579. doi:10.1242/jcs.232579

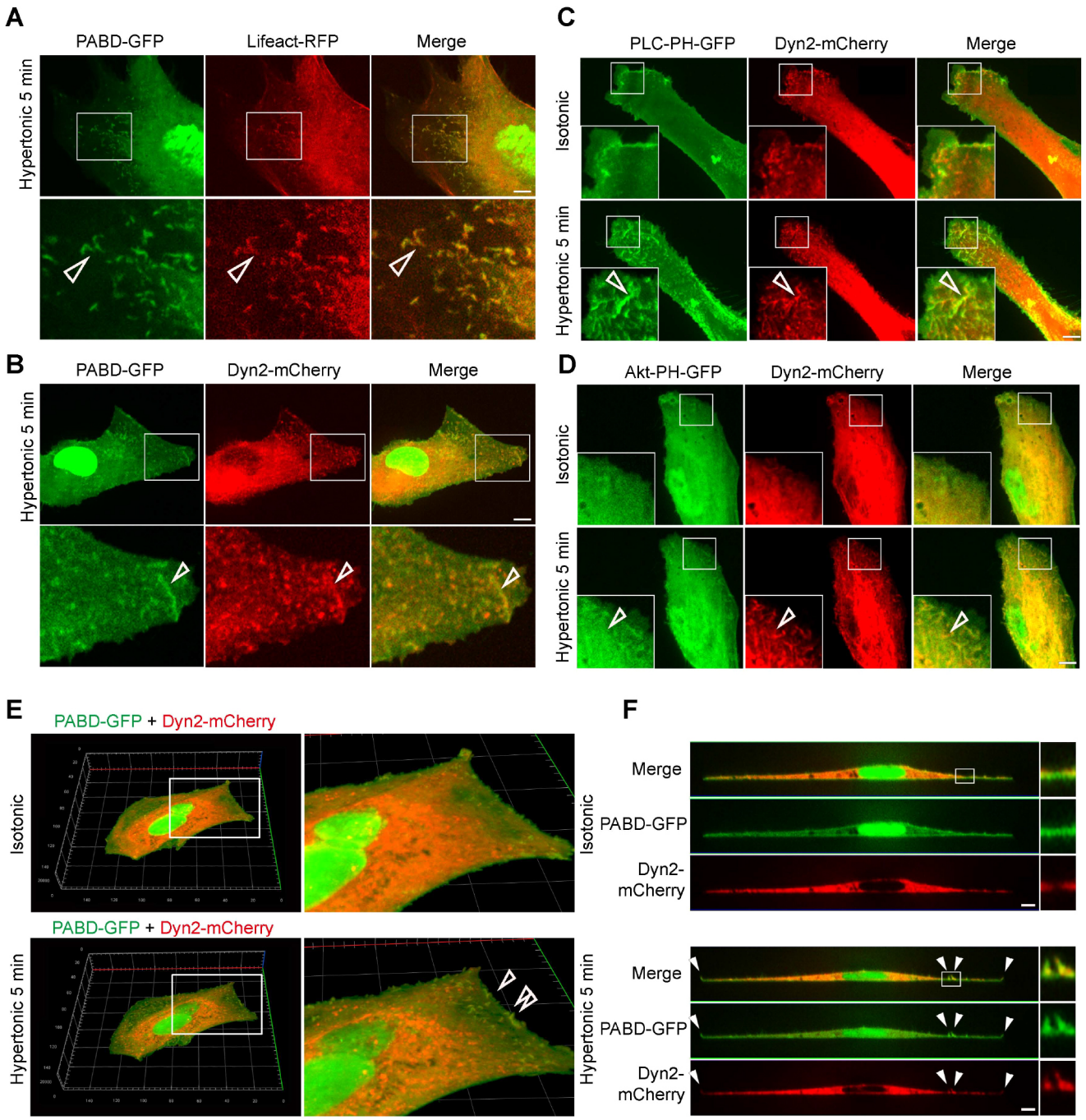

Fig. 2. Distribution of membrane proteins and lipids upon sudden decrease of PM tension. Myoblasts co-transfected with indicated plasmids were treated with hypertonic buffer for 5 min. (A–D) The tension drop-induced PA-rich ruffles (arrowheads) were examined with spinning disk confocal microscopy for its enrichment with F-actin (Lifeact–RFP), Dyn2, PI(4,5)P_2 (PLC-PH–GFP) and PI(3,4,5)P_3 (Akt-PH–GFP). Maximum projected images are shown. (E,F) 3D images of one myoblast incubated in isotonic and followed by hypertonic buffer. A PABD–GFP and Dyn2–mCherry co-transfected myoblast was imaged with *z*-stack spinning disk confocal microscopy before and after 5 min incubation in a hypertonic buffer. The 3D reconstructed images (E) and orthogonal views (F) are shown to illustrate dorsal membrane ruffling (open arrowheads in E and white arrowheads in F) upon tension drop. Scale bars: 10 µm.

treatments resulted in >25% cells containing more than three macropinosomes (Fig. 3C). Interestingly, compared with fetal bovine serum (FBS)-stimulated myoblasts, the hypertonic buffer-treated myoblasts showed a similar magnitude of dextran intensity increase (5-fold and 2.5-fold) and a comparable proportion of cells containing more than three macropinosomes (35.2±0.4% and 33.6±9.7%, mean±s.d.; Fig. 3B,C; Fig. S2E–G). However, the distribution of macropinosomes was distinct from that in FBS-stimulated cells, where they often cluster into ring-like structures that are reminiscent of platelet-derived growth factor-induced circular dorsal ruffles (Fig. S2E) (Yarar et al., 2007).

Similar to previous results, caveolin-1 was not enriched around the Rh-Dextran-labeled macropinosomes (Fig. 3D). Importantly, the decrease of PM tension induced by mechanical stretch and

Journal of Cell Science (2019) 132, jcs232579. doi:10.1242/jcs.232579

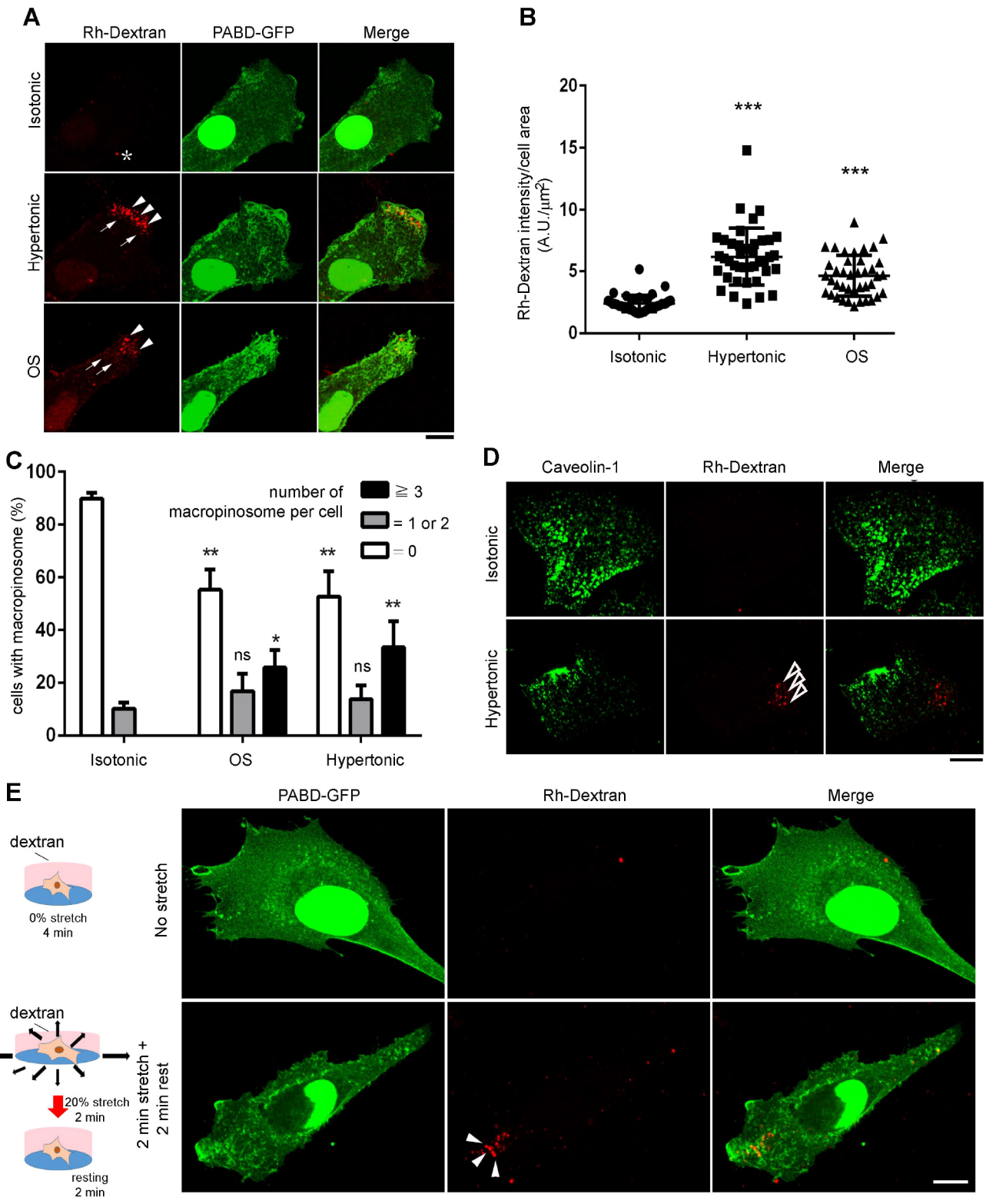

Fig. 3. See next page for legend.

relaxation also led to the formation of macropinosome in myoblasts (Fig. 3E). The results thus far suggest that an acute decrease of PM tension results in PA production, formation of membrane ruffling that are rich in actin, PI(4,5)P_2 and Dyn2, and, subsequently, macropinocytosis.

PLD2 is responsible for the PA production upon PM tension decrease

To examine whether PLD2 is responsible for the PA production induced by decreased PM tension, we first used a general PLD inhibitor, 1-butanol (Brown et al., 2007) to pre-treat myoblasts for

Fig. 3. Acute PM tension decrease induces macropinocytosis. (A) Macropinocytosis is induced upon hypertonic buffer or OS treatment. PABD–GFP-expressing myoblasts were incubated with indicated buffer plus 1 mg/ml Rh-Dextran. Buffers and conditions were 5 min isotonic, 5 min hypertonic or 2 min hypotonic (0.5× PBS without dextran) followed with isotonic (1× PBS with dextran) for OS. After wash and fixation, cells were imaged with confocal microscopy and the maximum intensity projection images were generated. Arrowheads and arrows indicate the macropinosome and other endocytic carriers, respectively. *, non-specific binding of dextran with the cell surface. (B) The Rh-Dextran intensity of cells upon tension manipulation as in A was quantified. (C) The number of macropinosomes (Rh-Dextran-containing vesicles larger than 0.5 µm in diameter) were quantified and divided into three populations as indicated. The percentage of each population were compared with the isotonic buffer-treated cells. Three independent experiments with over 160 total cells for each condition were analyzed and compared with isotonic-treated cells by one-way ANOVA. Results in B and C are mean±s.d. *P<0.05; **P<0.01; ***P<0.001; ns, not significant. (D) Distribution of macropinosomes and endogenous caveolin-1 in hypertonic buffer-treated cells. Open arrowheads indicate the macropinosome. (E) Mechanical stretch and relax induces macropinocytosis. PABD–GFP-expressing myoblasts were subjected to 0% or 20% radial stretch for 2 min and followed by 2 min rest in the presence of 1 mg/ml Rh-Dextran. After an intensive wash with PBS, myoblasts were fixed and imaged with confocal microscopy. Arrowheads indicate the macropinosomes. Scale bars: 10 µm.

10 min and then incubated the cells with hypertonic buffer (Fig. S3). After 10 min incubation with 0.1% 1-butanol in isotonic buffer, mild cell contraction and a diminished PABD–GFP signal on PM were observed (Fig. S3A). Further contraction of the cell was observed after hypertonic buffer treatment, yet no membrane ruffles were induced. By contrast, cells treated with the control alcohol (2-butanol) showed prominent membrane ruffles enriched with PABD–GFP and Dyn2–mCherry upon hypertonic buffer incubation (Fig. S3B). This result indicates that PLD activity is essential for the PA-rich membrane ruffles induced by decreased PM tension.

Mammalian cells express mainly two isoforms of PLD, PLD1 and PLD2, which are localized to intracellular membrane and PM, respectively. To examine the involvement of these two PLDs, we first monitored the distribution of PLD1 and PLD2 in cells treated with hypertonic buffer. While GFP–PLD1 remained intracellularly distributed in hypertonic buffer, GFP–PLD2 showed increased signals at dorsal membrane ruffles upon a decrease of PM tension (Fig. S4A). Image quantification results showed that the colocalization of GFP–PLD2 with Dyn2–mCherry ruffles was significantly higher than for GFP–PLD1 in hypertonic buffer-treated cells, with a colocalization ratio as 0.10±0.07 and 0.31±0.23, respectively (Fig. 4A,B). To further test the specific requirement of PLD2 activity upon decreasing PM tension, we used PLD1 or PLD2 specific inhibitors, UV0359595 and UV364739 respectively, to pre-treat the cells for 10 min in 1× PBS and followed by 5-min hypertonic buffer incubation together with the indicated inhibitor. Consistent with the subcellular localization results, we found that only PLD2 inhibitor blocked the membrane ruffling induced by decreased PM tension, but not in PLD1 inhibitor-treated cells (Fig. 4C; Fig. S4B). Similarly, only the PLD2 inhibitor reduced the number of macropinosomes in cells treated with hypertonic buffer (Fig. 4D; Fig. S4C).

To substantiate the specific requirement of PLD2 in decreased PM tension-induced macropinocytosis, we knocked down (KD) either PLD1 or PLD2 with two different lentiviral shRNA sequences. Similar to the results of PLD inhibitors, we observed a significant reduction of membrane ruffles and macropinosome formation in PLD2 KD, but not in PLD1 KD cells (Fig. 4E,F; Fig. S4D). It is worth noting that when PLD1 or PLD2 were knocked down, the expression of the other isoform was slightly increased (Fig. S4E,F), indicating a compensatory expression and adaptation phenomenon of cells with PLD depletion.

Taken together, these results suggest that decreased PM tension induces PA production and macropinocytosis via PLD2 activity. Notably, the intracellular GFP–PLD1 vesicles were diminished upon tension surge concurrently with increased GFP–PLD1 signals on PM (Fig. S5A), whereas GFP–PLD2 became less enriched on PM with hypotonic buffer treatment (Fig. S5B). These results indicate that both PLDs respond to PM tension change and may explain why both an increase and a decrease of PM tension causes an increase of total PA amount (Fig. S1B).

Lipid microdomain responds to tension alteration

Lipid microdomains or nanodomains have been reported as mechanosensors that could be disrupted chemically or mechanically (Oglęcka et al., 2014; Petersen et al., 2016). We wondered whether the integrity of lipid domains might be affected by membrane tension *in vitro* and *in vivo*. To directly observe the effect of membrane tension on lipid microdomains, we utilized giant unilamellar vesicles (GUVs), a commonly used membrane template for studying lipid phase separation (Liu and Fletcher, 2006; Wesołowska et al., 2009), to monitor the size of different lipid phases with the L_o (liquid-ordered) domains labeled with TopFluor cholesterol and L_d (liquid-disordered) domains labeled with Rhodamine-conjugated phosphatidylethanolamine (rhodamine–PE). In GUVs composed of DOPC:DPPC:cholesterol:TopFluor cholesterol:rhodamine–PE with molar ratio of 39:39:20:1:1, we observed phase separation with several L_o domains (~3–10 per GUV) when the GUVs were incubated in isotonic buffer (Fig. 5A; Movie 3). Strikingly, when GUVs were incubated in hypotonic buffer, those L_o domains merged into one large domain with numerous small L_o domains continuously formed and fused together (Fig. 5A; Movie 4). By contrast, L_o domains became smaller in hypertonic buffer where GUVs on a coverslip resemble flatten tires (Fig. 5A; Movie 5). Similar phenomenon could also be observed with the GUV first incubated in an isotonic buffer that was then adjusted into a hyper- or hypotonic buffer (Fig. S6A,B). Notably, it is challenging to image a GUV with compromised phase separation upon hypertonic buffer addition since the water flow preferentially induces membrane deformation on a flaccid GUV (Fig. S6C). These results convincingly showed that membrane tension affects the integrity of the lipid microdomain on a model membrane.

To test whether the disintegration of lipid microdomain could be observed in a cell upon a decrease of PM tension, we utilized Alexa Fluor 594-conjugated cholera toxin B (CTB-AF 594), which binds to the sphingolipid GM1 to label lipid microdomains. Upon different osmotic buffer treatments, cells were fixed and stained with CTB-AF 594 without permeabilization. After intensive washes, we used stimulated emission depletion (STED) microscopy to image the ventral surface of myoblasts and found the CTB clusters seemed to be less compact in hypertonic buffer-treated cells (arrowheads in Fig. 5B).

PLD2 is localized to lipid domain via its palmitoylation (Xie et al., 2002), and thus is segregated from its substrate (PC) and activator (PIP_2) without an inducer. To visualize the effect of PM tension of PLD2 distribution, we used STED microscopy to image GFP–PLD2 in hypertonic or hypotonic buffer-treated cells and quantified the area of the GFP–PLD2 nanodomain (in nm^2) with MetaMorph software. Although the hypertonic buffer-treated cells had a similar size of GFP–PLD2 nanodomains to those in control

Journal of Cell Science (2019) 132, jcs232579. doi:10.1242/jcs.232579

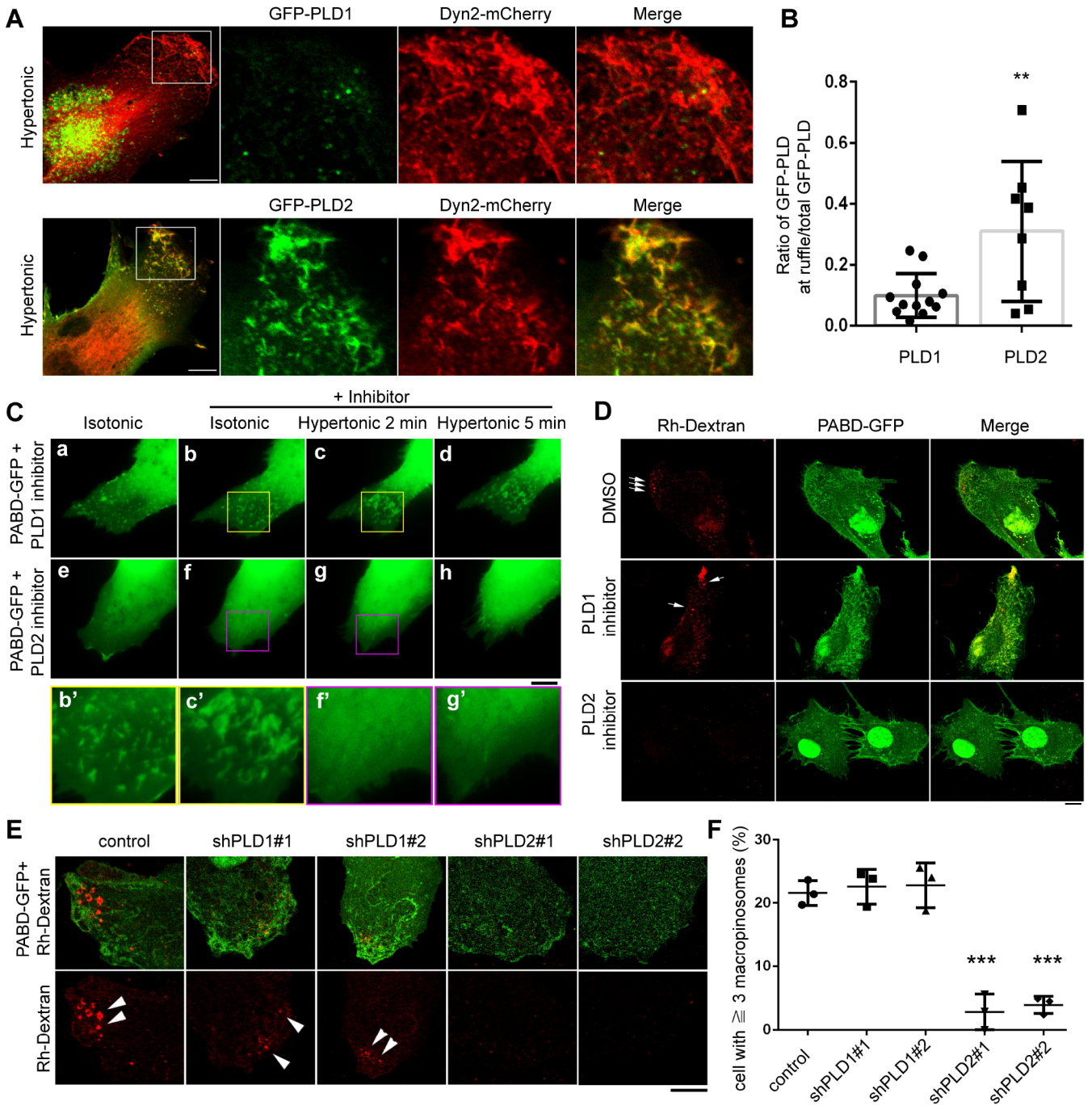

Fig. 4. PLD2 is required for membrane ruffling and macropinocytosis induced by an acute decrease in PM tension. (A) PLD1 and PLD2 distribution upon membrane tension drop. Myoblasts expressing GFP–PLD1 or GFP–PLD2 together with Dyn2–mCherry were imaged with confocal microscopy after hypertonic buffer treatment. The colocalization ratio for PLD with ruffles labeled by Dyn2–mCherry were quantified with ZEN software (B). 10 cells were analyzed for each condition and compared by *t*-test. (C,D) Effect of PLD inhibitors on tension drop-induced membrane ruffles and macropinocytosis. PABD–GFP-expressing myoblasts were pretreated with indicated PLD inhibitors, (500 nM for 10 min in 1× PBS), and followed by inhibitor-containing hypertonic buffer for another 5 min (C) or Rh-Dextran-containing hypertonic buffer and OS treatment (D). Live-cell imaging (C) or confocal imaging on fixed cells (D) were utilized. (E,F) Macropinocytosis in PLD-knockdown cells. PABD–GFP-expressing, PLD KD myoblasts were monitored with Rh-Dextran internalization upon hypertonic buffer treatment. The population of cells with more than three macropinosomes (diameter ≥0.5 µm) were quantified and compared with control cells (F). 120 cells from three independent experiments of each condition were scored and compared with control cells by one-way ANOVA. Results in B and F are mean±s.d. ***P*<0.01; ****P*<0.001. Arrows and arrowheads in D and E highlight Rh-dextran containing macropinosomes. Scale bars: 10 µm.

cells, 13,177±17,192 and 13,434±18,880 nm^2, respectively, hypotonic buffer treatment led to a significantly increased area of GFP–PLD2 nanodomains, 16,525±30,611 nm^2 (Fig. 5C,D). Interestingly, when analyzing the distribution of the total GFP–PLD2 nanodomains, we noticed that the larger-sized domains seemed slightly smaller in hypertonic buffer-treated cells (Fig. 5D). To further look into the effect of PM tension of larger-sized PLD2 nanodomains, we compared the size distribution of the top 10% of GFP–PLD2 nanodomains and found a significant reduction in hypertonic buffer-treated cells relative to isotonic

Journal of Cell Science (2019) 132, jcs232579. doi:10.1242/jcs.232579

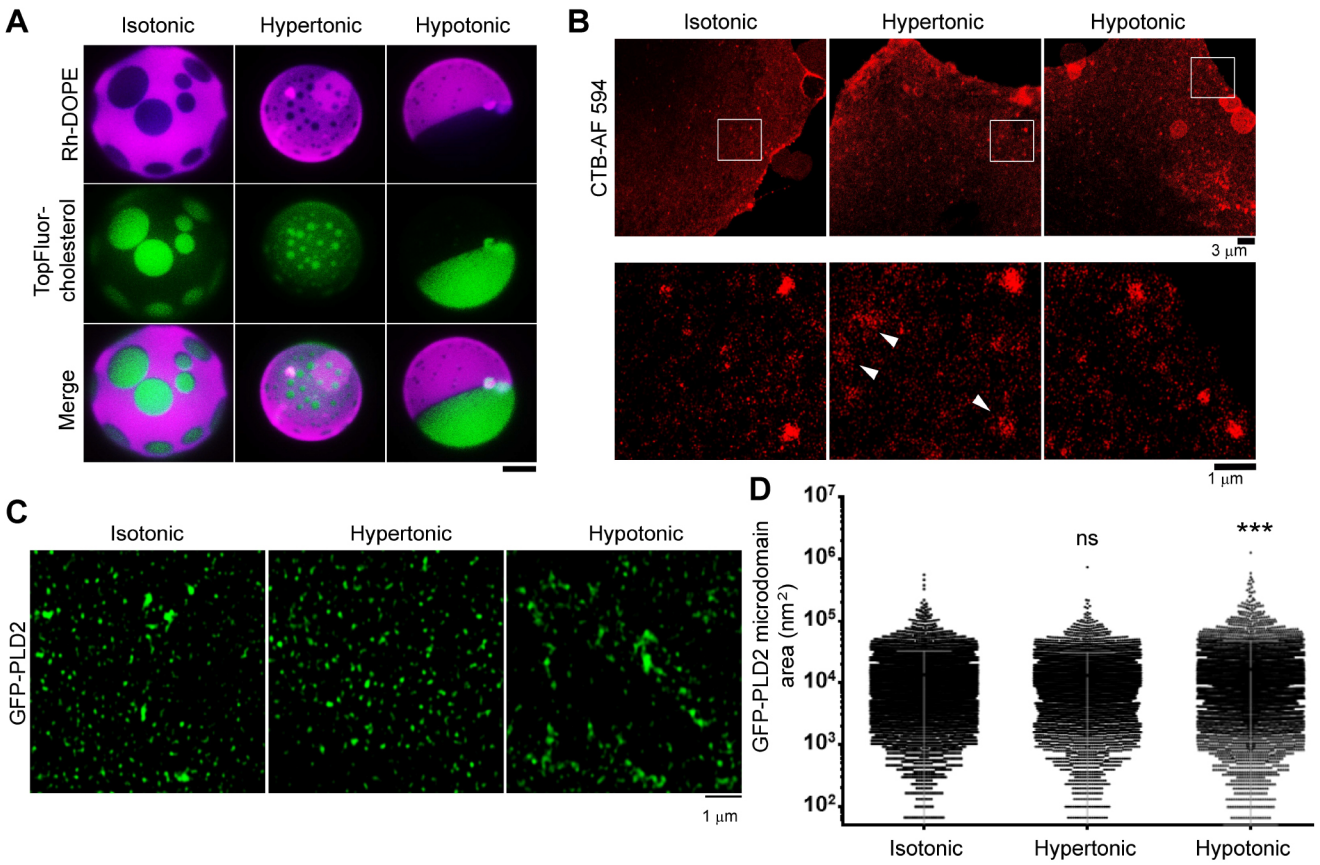

Fig. 5. Lipid microdomain disintegration upon tension decrease. (A) Effects of tension changes on lipid phase separation. GUVs with TopFluor cholesterol (green) and Rhodamine–PE (magenta), to label the L_o and L_d domains, respectively, were subjected to iso- (400 mM), hyper- (500 mM) or hypotonic (300 mM) glucose buffers and imaged with inverted epi-fluorescence microscopy. Scale bar: 10 µm. (B) Effects of hypertonic or hypotonic buffer treatment on CTB-labeled lipid microdomains in cells. Myoblasts were treated with the indicated buffers and followed by fixation, CTB staining and STED microscopy. Arrowheads indicate the disintegrated CTB microdomains. (C) Effects of hypertonic or hypotonic buffer treatment on GFP–PLD2 nanodomains in cells. GFP–PLD2-expressing C2C12 were treated with indicated buffers and followed by fixation and STED microscopy. (D) The size of GFP–PLD2 nanodomain was quantified with MetaMorph software. For each condition, over 6000 microdomains from six cells were analyzed and compared with isotonic buffer treated cells by one-way ANOVA. ***P<0.001; ns, not significant.

buffer (46,277±35,970 and 50,048±40,627 nm^2, with P=0.04, one-tailed t-test) (Fig. S6D). In addition, we performed super-resolution imaging by stochastic optical reconstruction microscopy (STORM), analyzed with the ThunderSTORM plugin in ImageJ and found partial colocalization between GFP–PLD2 and CTB in hypertonic buffer-treated cells (Fig. S6E). Together, these results suggest that membrane tension facilitates lipid phase separation, thus GFP–PLD2 nanodomains may disintegrate into smaller ones upon PM tension decrease.

Acute decrease of PM tension in myotube induces macropinosome formation

Given the results above, we have identified a previously underappreciated mechanotransduction pathway based on PM tension alteration and leading to PA production. We thus wondered whether this pathway would be pronounced in tissues with perpetual mechanical stresses.

Skeletal muscle is constantly exposed to mechanical stress in our body and thus has been intensively studied for its ability to cope with increased PM tension. Muscle cells are equipped with robust caveolae structures that could quickly disassemble when membrane tension increases in order to release membrane reservoir and thus relieve the tension surge (Lo et al., 2015; Sinha et al., 2011). However, little is known about how muscle cells react upon a rapid decrease in PM tension. We thus examined the response of C2C12-derived myotubes encountering hypertonic buffer (1× PBS + 150 mM sucrose for 5 min) or OS treatment (2 min 0.25× PBS incubation followed by 2 min 1× PBS recovery), and found significant amounts of dextran-containing macropinosomes in the myotubes with an acute decrease in PM tension (Fig. S7A). Remarkably, the macropinosomes induced by OS were much larger than the ones in hypertonic buffer-treated myotubes and could be observed under light microscopy (Fig. 6A; Fig. S7B). This is probably due to the increase of membrane area caused by caveolae disassembly during hypotonic treatment (black arrow in Fig. 6A) and thus results in more-pronounced macropinosomes than cells subjected to hypertonic buffer incubation.

Using time-lapse microscopy, we found that the OS-induced dextran-positive macropinosomes were also enriched with PA (Fig. 6B). Similar to what was seen in myoblasts, the OS treatment in myotubes also induced membrane ruffling and the enrichment of F-actin at PA-positive macropinosomes (Fig. 6C,D; Movies 6, 7). It is worth noting that macropinosomes could be initiated from the cell–substratum contact site in myotubes (white arrow in Fig. 6C), and not only from the dorsal surface.

Furthermore, the muscle isoform of caveolin, caveoiln-3, did not colocalize with PA at the macropinosomes induced by OS

Journal of Cell Science (2019) 132, jcs232579. doi:10.1242/jcs.232579

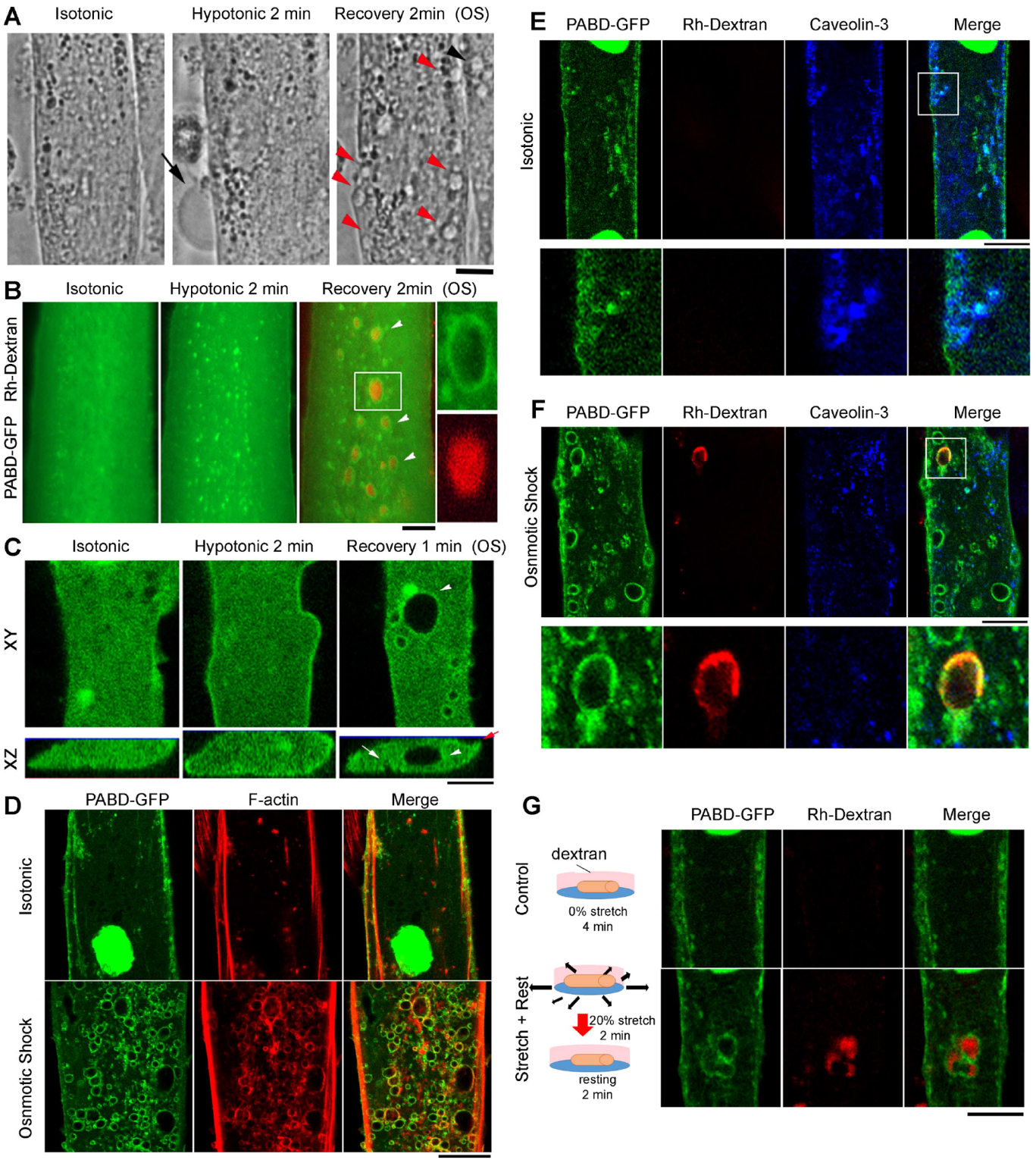

Fig. 6. Acute PM tension decrease induces macropinocytosis in myotubes. (A) Morphology of myotubes treated with isotonic buffer (Aa), hypotonic buffer (Ab) and followed by isotonic buffer recovery (Ac). Phase-contrast microscopy images were captured with inverted fluorescence microscopy. The black arrow indicates a membrane bleb from cell swelling, and the red and black arrowheads point to macropinosomes induced by tension drop. (B,C) OS-induced macropinosomes are enriched with PA in OS-treated myotubes. Live-cell imaging of PABD–GFP-expressing myotubes captured with wide-field (B) or spinning disk confocal (C) microscopy. (B) Cells were incubated in isotonic buffer, hypotonic buffer and recovery isotonic buffer containing 1 mg/ml Rh-Dextran for 2 min with an intensive wash. Insets are magnified images from the boxed areas. White arrowheads indicate the sealed macropinosomes. (C) *xy* or *xz* views of single-plane confocal images are shown. The red arrow indicates a membrane ruffle, the white arrow and arrowheads indicate the intermediate and the sealed macropinosomes, respectively. (D–F) Distribution of F-actin and caveolin-3 in myotubes with OS treatment. PABD–GFP-expressing myotubes, with or without OS treatment, were stained with Rhodamine–phalloidin (D) or for caveolin-3 (E,F). Single-plane confocal images are shown. Lower panels in E and F show a magnification of the boxed region. (G) Radial stretch induces macropinosome formation in myotubes. PABD–GFP-expressing myotubes incubated in 1 mg/ml Rh-Dextran medium were subjected to 0% or 20% radial stretch for 2 min and followed by 2 min resting (0% stretch). After an intensive wash with PBS, myotubes were fixed and imaged with confocal microscopy. Scale bars: 10 µm.

Journal of Cell Science (2019) 132, jcs232579. doi:10.1242/jcs.232579

(Fig. 6E,F). Here, we intentionally started to wash the cells upon 1 min of OS treatment and fix them ∼2 min after recovery to specifically observe the early stage of macropinocytosis, thus the macropinosomes were not fully filled with dextran (Fig. 6F). Importantly, similar results could be observed in myotubes upon mechanical stretch and relaxation, but not in the control myotubes which were incubated in dextran without stretching (Fig. 6G). These results demonstrate that, similar to OS treatment, the acute decrease in PM tension induced by cell stretching and relaxation also triggers PA production and macropinocytosis in myotubes. We hereafter utilized OS-treated myotubes to observe the kinetics and contribution of PLD to the macropinocytosis induced by a decrease of PM tension in myotubes.

PLD activity is required for the formation of macropinosome induced by decreased PM tension in myotube

Next, we tested whether PLD is also responsible for the macropinocytosis induced by the decrease of PM tension in myotubes. Interestingly, PLD1–GFP distributed both on the PM and in intracellular vesicles in myotubes and was partially distributed to macropinosomes after OS, whereas PLD2 was localized at the PM in isotonic conditions and became enriched at macropinosomes upon OS treatment (Fig. 7A,B). Consistent with these observations, OS-induced macropinosome formation in myotubes could only be blocked by the dual PLD1/PLD2 inhibitor FIPI, or the combined treatment of PLD1 and PLD2 inhibitors (Fig. 7C–E; Fig. S7B). Taken together, these data indicate that the decreased PM tension–PLD–macropinocytosis pathway is prominent in myotubes, and both PLD1 and PLD2 are involved.

Distinct from the macropinocytosis in myoblasts, where macropinosomes were enriched with Dyn2–mCherry, we did not observe obvious enrichment of Dyn2–mCherry at the OS-induced macropinosomes (Fig. 7A,B). We thus carefully examined the kinetics of distribution of Dyn2–mCherry and PABD–GFP in myotubes subjected to OS, and we found that Dyn2–mCherry only enriched at the PABD–GFP ring at the PM in the early stage of OS treatment (Fig. 7F, inset). Remarkably, only when the macropinosome was formed above the nucleus where much less cytosolic signals exist could the Dyn2–mCherry observed on the PM, potentially representing the early stage of macropinocytosis (Fig. 7F). In addition, different from the PA-labeled macropinosomes, which could remain for more than 10 min in myotubes, the Dyn2–mCherry ring quickly disappeared from the PM upon OS treatment, suggesting the dissociation of Dyn2 after macropinosome pinching off from the PM (Antonny et al., 2016).

PA is known to promote actin polymerization through $PI(4,5)P_2$ production and Rac activation (Liu et al., 2013). However, it has not been addressed whether PA could affect the activity of Dyn2, which is a membrane fission GTPase essential for phagocytosis and macropinocytosis (Liu et al., 2008; Marie-Anaïs et al., 2016). To test that, we analyzed the activity of purified recombinant Dyn2 on lipid templates containing different concentrations of PA. We found that both the GTPase activity and the membrane fission ability of Dyn2 increase in a PA-dependent manner (Fig. S8A,B). Furthermore, Dyn2 assembled into a more-ordered helical structure in PA-containing liposomes (Fig. S8C). Together, these results suggest that PA could promote macropinocytosis via not only actin polymerization but also by stimulating the macropinosome pinching off from PM.

DISCUSSION

Macropinocytosis is a unique endocytic pathway initiated by biochemical stimulations to efficiently uptake nutrients, terminate signaling or internalize viruses (Buckley and King, 2017). In this study, we identified a PLD-dependent pathway for macropinocytosis initiation that is induced by an acute decrease of PM tension, followed by PLD2 nanodomain disintegration, increased PLD2 activity, augmented PA production and membrane remodeling (Fig. 8). This mechanotransduction pathway contributes differently among cell types and is relatively pronounced in myotubes. Our discovery thus provides a molecular interpretation for how cyclic stretching and relaxation would lead to PLD activation, which subsequently stimulates mTORC1, the critical complex coordinating cell growth and environmental cues (Hornberger et al., 2006, 2007; Lin and Liu, 2019).

Several endocytic pathways have been reported to be induced by a sudden decrease of PM tension, including the CLIC/GEEC pathway, vacuole-like dilation and GRAF-1-dependent endocytosis (Holst et al., 2017; Kosmalska et al., 2015; Thottacherry et al., 2018). Despite the similarity in morphology, the dependency on PLD activity and the enrichment of actin found in macropinocytosis induced by decreased PM tension in myoblasts is distinct from the ATP- and actin-independent vacuole-like dilation found in mouse embryonic fibroblasts upon cell volume decrease (Kosmalska et al., 2015). Instead, the macropinocytosis induced by decreased PM tension is reminiscent of activity-dependent bulk endocytosis (ADBE), the dominant mode of synaptic vesicle endocytosis during intense neuronal activity (Clayton and Cousin, 2009). Therefore, it is tempting to speculate that the decreased PM tension–PLD2 activation–macropinocytosis pathway may underpin ADBE, which couples massive synaptic vesicle exocytosis and quick recycle of these synaptic components. Together, given that more than one endocytic processes would be enhanced upon the decrease of PM tension (Fig. 3) and different strategies of PM tension reduction would lead to distinct cell remodeling pathways (Holst et al., 2017; Kosmalska et al., 2015; Thottacherry et al., 2018), we believe that cells could react towards decreased PM tension in a versatile and flexible way, depending on cell types and magnitude of tension alteration as well as cell–matrix interaction.

Lipid domains are well perceived as a signaling platform given their enrichment of unique receptors, yet they have not been reported to be involved in macropinocytosis. While PLD1 has been found to be necessary for EGF-induced macropinocytosis (Haga et al., 2009), here we find that the PLD2 nanodomain serves as a mechanosensor that transduces the mechanical cue into biochemical signals to initiate PLD2 activity and macropinosome formation.

The effect of membrane tension on the coarsening of lipid domains *in vitro* has been largely studied and modeled theoretically (Akimov et al., 2007; Chen and Santore, 2014; Hamada et al., 2011; Oglęcka et al., 2014; Portet et al., 2012; Ursell et al., 2009). Thus, it is believed that the membrane tension sensitivity of lipid domain may arise from (1) the increase of line tension when membrane tension rises (Akimov et al., 2007), or (2) the kinetics of domain coalescence affected by membrane tension (Ursell et al., 2009). Line tension is the boundary energy between the L_o and L_d domains arising from the difference of their membrane thickness, also known as hydrophobic mismatch. Therefore, it is intuitive to imagine that membrane with lower tension would have lower boundary energy, thus the total circumference of L_o could increase, that is, a larger number of L_o domains with smaller diameters (Fig. 8). We thus hypothesize that PLD2 catalyzes reactions at the boundary of lipid nanodomains, and the effect of decreased PM tension on lipid domain would increase the amount of phase boundaries thus leads to higher PLD2 activity.

The activity of PLDs has been reported to be sensitive to mechanical stress, such as mechanical stretching, membrane tension surge or osmotic stress (Diz-Muñoz et al., 2016; Hornberger et al.,

Journal of Cell Science (2019) 132, jcs232579. doi:10.1242/jcs.232579

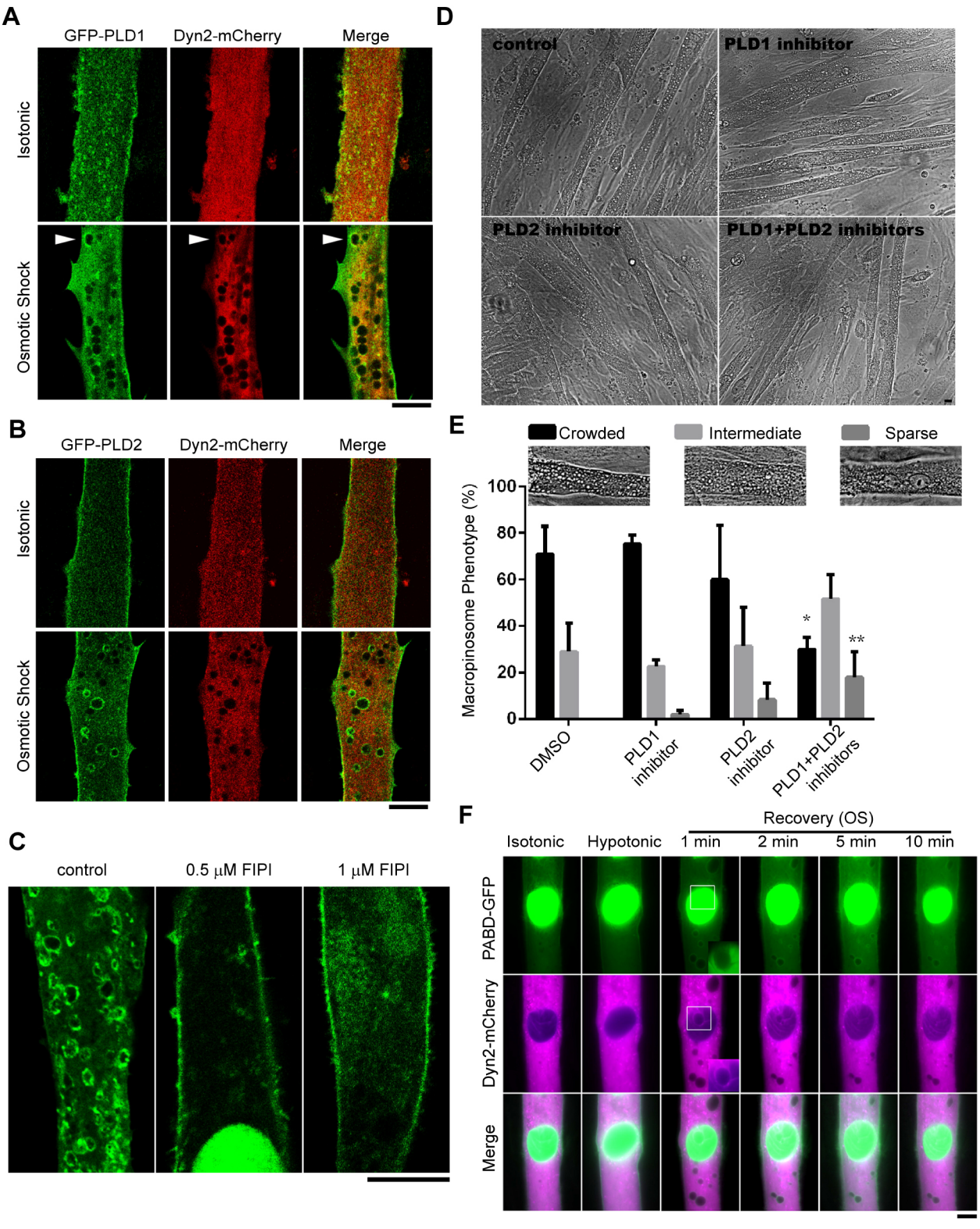

Fig. 7. See next page for legend.

2006; Lin and Liu, 2019; Tomassen et al., 2004). However, how exactly PLD is activated upon mechanical stimulation remains unclear. Here, we found that PLD1 and PLD2 distribute differently and react to distinct PM tension alterations in myoblasts. Nonetheless, it is puzzling that both an increase and a decrease of PM tension result in elevated total amount of PA, yet result in different cellular outcomes: actin depolymerization or polymerization, respectively (Diz-Muñoz et al., 2016; Tsujita et al., 2015). Since the subcellular location of PA and its surrounding proteins determine where and in what kind of cellular event it would participate (Colley et al., 1997; Du et al., 2004; Teng et al., 2015; Yang and Frohman, 2012), it is plausible that elevated PA in different membrane compartments would trigger

Fig. 7. Both PLD1 and PLD2 contribute to the macropinosome formation in OS-treated myotubes. (A,B) Distribution of PLD1 and PLD2 in OS-induced macropinosomes. C2C12-derived myotubes expressing GFP–PLD1, GFP–PLD2 and Dyn2–mCherry were treated with isotonic buffer or OS and followed by fixation and image acquisition with confocal microscopy. Single-plane focal images are shown. Arrowheads, PLD1-enriched macropinosomes. Scale bars: 10 µm. (C–E) Effects of PLD inhibitors on OS-induced macropinosome formation. Myotubes were pre-treated with the indicated inhibitors (0.5 µm or 1 µm of FIPI, 1 µm PLD1 and/or 1 µm PLD2 inhibitor) for 10 min, followed by OS treatment together with the indicated inhibitors. Fixed, confocal images are shown in C, and phase contrast images are shown in D. The phenotypes were analyzed and divided into three categories: crowded (macropinosome with diameter>2 µm with density above 27/10,000 µm^2), intermediate (1.5~27 macropinosomes/10,000 µm^2) and sparse (below 1.5 macropinosomes/10,000 µm^2) as shown as the mean±s.d. in graph (E). Data from three independent experiments with n>100 myotubes for each condition were compared to DMSO-treated control by one-way ANOVA. *P<0.05; **P<0.01. (F) Kinetic distribution of PABD–GFP and Dyn2–mCherry in an OS-treated myotube. Boxed areas were magnified and adjusted for green fluorescence intensity to better observe the macropinosome on top of a nucleus (shown in the insets).

distinct cellular processes. Further studies are needed to elucidate the feedback regulation of PM tension, PA production, membrane trafficking and actin polymerization in order to fully decipher the complexity of this network.

The mechanotransduction pathway we discovered here supports the concept that PM tension is an integrator for biochemical and physical cues to regulate membrane trafficking and actin organization (Diz-Muñoz et al., 2013). By examining the molecular basis of this regulatory network, we uncovered the mechanisms underpinning membrane organization and PLD activity. Given the ubiquitous nature of membrane tension in the eukaryotic cells, we suspect there must be more molecules sensing and/or regulated by PM tension. Our findings pave the way for future studies of the mechanical regulation on membrane and cell physiology.

MATERIALS AND METHODS

Cell culture, transfection and infection

Mouse-derived C2C12 myoblasts (American Type Culture Collection, CRL-1772) were cultured in growth medium [GM; DMEM supplemented with 2 mM L-glutamine, 1 mM sodium pyruvate, antibiotics and 10% fetal bovine serum (Gibco)]. To induce differentiation, C2C12 cells were seeded onto laminin (Invitrogen)-coated glass-bottom dishes (MatTek) or coverslips in GM, grown to 90% confluency, and then switched to differentiation medium (DM), which is the same as GM but with 2% horse serum (Gibco). This time point was considered as day 0 of differentiation. For transfection, cells at 70% confluency were transfected with the desired DNA constructs using Lipofectamine 3000 (Invitrogen), as recommended by the manufacturer. Constructs used for transfections are listed in Table S1.

For PLD knockdown experiments, lentiviruses with shRNA sequences [5′-CCCAATGATGAAGTACACAAT-3′ (#1) or 5′-GCTTGGTAATAA-GTGGATAAA-3′ (#2) for PLD1; 5′-CCTTCCTGTCACCAAGTTCAA-3′ (#1) or 5′-CATGTCTTTCTATCGCAATTA-3′ (#2) for PLD2] were prepared. C2C12 myoblasts were infected with control- or PLD-shRNA-containing lentiviruses and selected with 2 µg/ml puromycin for 3 days then subjected to transfection and osmotic buffer treatments.

Reagents

The PLD1 inhibitor UV0359595 was purchased from Cayman Chemical. PLD2 inhibitor UV0364739 and FIPI were from Tocris Bioscience. Rh-dextran, CTB-AF 647 and CTB-AF 594 were from Invitrogen. The concentrations and incubation times of inhibitors have been stated in the relevant figure legends. Anti-PLD2 antibody (ab86437, immunoblotting with 1:250 dilution) was purchased from Abcam, anti-α-tubulin antibody (T6074, immunoblotting with 1:5000 dilution) was from Sigma-Aldrich, anti-PLD1 (#3832, immunoblotting with 1:1000 dilution) and anti-caveolin-1 (#3267, immunostaining with 1:400 dilution) antibodies were from Cell Signaling Technology, anti-caveolin-3 antibody (sc-5310, immunostaining with 1:200 dilution) was from Santa Cruz Biotechnology. All lipids were purchased from Avanti Polar Lipids. For indirect immunofluorescence staining, cells were fixed and permeabilized as previously described (Liu et al., 2008), and then stained with indicated antibodies at room temperature for 1 h. For protein expression analysis, cell lysates were harvested after indicated lentiviral infection and puromycin selection. Cell lysates were then subjected to immunoblotting analysis as previously described (Du et al., 2004). For indirect immunofluorescence staining, cells were fixed and permeabilized as previously described (Liu et al., 2008), and then stained with indicated antibodies at room temperature for 1 h.

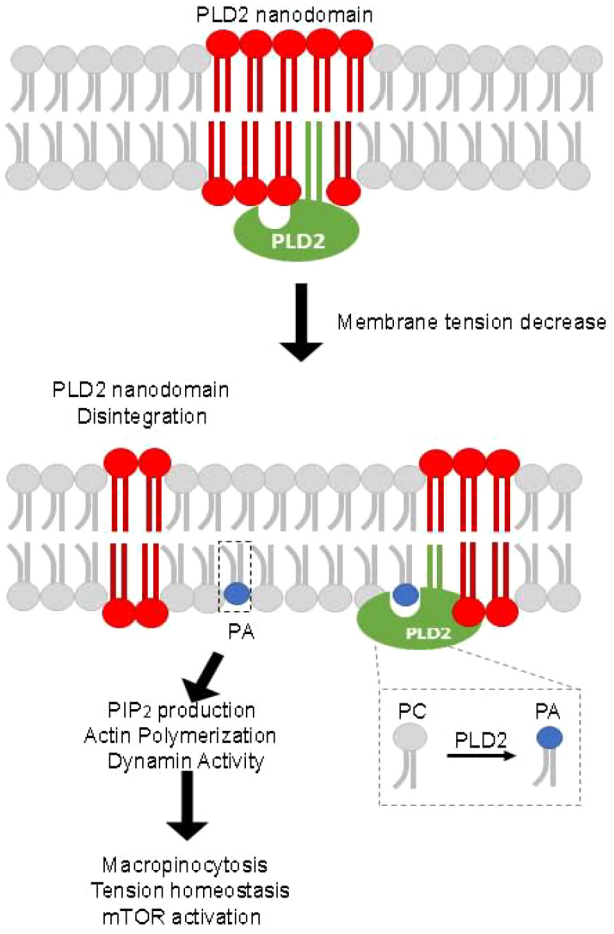

Fig. 8. Model of PLD2 nanodomain disintegration and macropinocytosis caused by a decrease in PM tension. Under normal tension, lipid phase separation results in lipid-ordered domain formation and thus segregates PLD2 from its activator PI(4,5)P_2 as well as its substrate PC (upper panel). When PM tension is reduced, the size of lipid nanodomain is also reduced, thus allowing more PLD2 to access its activator and substrate. The production of PA on the PM leads to PI4P-5 kinase activation to generate PI(4,5)P_2 and promotes higher PLD activity, actin polymerization, Dyn2 activation and, subsequently, membrane ruffling and macropinocytosis. PA enrichment on the macropinosome could also recruit and activate mTORC1 thus stimulates the growth of muscle.

Microscopy

For live-cell microscopy, cells transfected with the DNA constructs of interest were seeded on glass-bottom dishes (MatTek) and imaged with a Zeiss inverted Axio Observer Z1 or spinning disc confocal microscope (Zeiss Observer SD) at 37°C with a 63×, 1.35 NA oil-immersion objective. To image fixed cells, sample slides were observed with confocal LSM700 microscope with a 63×, 1.35 NA oil-immersion objective (Zeiss).

For super-resolution microscopy, we used STED to image cells upon hyper- or hypo-osmotic shock. Cells treated with different osmotic buffers

and followed by fixation and Alexa Fluor 594-CTB (Invitrogen) staining, were mounted in ProLong Gold antifade reagent (Invitrogen) and imaged under Leica TSC SP8 STED with a 100×, 1.4 NA oil objective. Images were acquired by using a 488 or 594 nm excitation laser with a 592 nm or 660 nm depletion laser and a Hybrid Detector (Leica HyD).

PA measurement

Total PA content was measured with a coupled enzymatic reaction assay (total phosphatidic acid assay kit, Cell Biolabs, Inc.). Briefly, cells treated with buffers of different osmolarities were scraped from dishes. While 10% of the samples were used for protein concentration analysis, the rest of the samples were subjected to total lipid extraction with methanol and chloroform. After drying with a SpeedVac, the lipid film was dissolved and the amount of PA was determined by a fluorometric assay that first hydrolyzed PA to glycerol-3-phosphate by lipase. Next, glycerol-3-phosphate product was oxidized by glycerol-3-phosphate oxidase, producing hydrogen peroxide which reacted with a fluorometric probe with excitation and emission wavelength at 530–560 nm and 585–595 nm, respectively. The PA amount was determined as fluorescence intensity (as arbitrary units) normalized to protein amount (μg).

Macropinocytosis assay

To monitor macropinocytosis, myoblasts or myotubes were incubated with indicated osmotic buffers containing 1 mg/ml Tetramethylrhodamine dextran (Thermo Fisher Scientific). After washing five times in PBS, cells were fixed and imaged by confocal microscopy. To monitor macropinocytosis in myotubes upon cell stretching, myoblasts were seeded on laminin-coated flexcell silicon dishes and were induced to differentiate for 5 days after PABD–GFP transfection. Day-5 differentiated myotubes were incubated in DM medium containing 1 mg/ml Rh-Dextran and subjected to radial stretching of 2 min at 20% extension and followed by 2 min resting. After intensive washing, fixation and mounting, cells were imaged by confocal microscopy.

GUV preparation

For GUV formation, lipid mixtures (DOPC:DPPC:cholesterol:Rhodamine-PE:Topfluor-cholesterol at 39:39:20:1:1) were dried on an indium tin oxide (ITO)-coated glass slide and electroformation was conducted via applying 3.5 V alternating current for 3 h in 400 mM sucrose at 50°C. To monitor the effect of tension changes on lipid phase separation, freshly prepared GUVs were subjected to isotonic buffer (400 mM glucose), hypertonic buffer (500 mM glucose) or hypotonic buffer (300 mM glucose) and imaged with inverted fluorescence microcopy immediately.

Cell stretching and imaging

C2C12 cells seeded on laminin-coated BioFlex Culture Plate (Flexcell) was transfected with PABD–GFP and where then either induced to differentiation into myotubes by DM incubation, or not. To monitor macropinocyrosis, Rh-Dextran was added into the medium to reach 1 mg/ml, and cells were subjected to static, radial stretching with 20% strain with a Flexcell FX-5000T Tension System for 2 min and followed by no stretching for 2 min; whereas control cells were incubated in Rh-Dextran-containing medium for 4 min without mechanical stress. Samples were then washed with PBS five times, fixed with 4% formaldehyde for 30 min, cut from the plates and mounted with mounting medium on a coverslip. PABD–GFP and Rh-Dextran signals were imaged with confocal microscopy (Zeiss, LSM700).

Statistical analysis

Quantitative data were expressed as mean±s.d. of at least three independent experiments. All data were analyzed with one-way ANOVA followed by Dunnet's post-hoc test or Student's *t*-test. $P<0.05$ was considered as statistically significant. *P*-values are indicated as $*P<0.05$; $**P<0.01$; $***P<0.001$.

Acknowledgements

We thank Dr Do Sik Min (Pusan National University) for the GFP-PLD1 and GFP-PLD2 plasmids. We are grateful to Dr Chau-Hwang Lee (Academia Sinica) for the assistance with GUV preparation.

Competing interests

The authors declare no competing or financial interests.

Author contributions

Conceptualization: J.L., S.-S.L., J.J., A.P.L., Y.-W.L.; Methodology: J.L., M.-C.C., S.-S.L., J.J., Y.-A.S., T.-L.H., Y.-C.C., Y.-W.L.; Formal analysis: J.L., S.-S.L., J.J., Y.-W.L.; Investigation: J.L., M.-C.C., S.-S.L., J.J., Y.-A.S., T.-L.H., Y.-C.C., Y.-W.L.; Data curation: J.L., M.-C.C., S.-S.L., J.J., Y.-W.L.; Writing - original draft: A.P.L., Y.-W.L.; Writing - review & editing: J.L., A.P.L., Y.-W.L.; Supervision: A.P.L., Y.-W.L.; Project administration: A.P.L., Y.-W.L.; Funding acquisition: A.P.L., Y.-W.L.

Funding

This work was supported by the Ministry of Science and Technology (grant 107-3017-F-002-002) and National Taiwan University (grant NTU-CDP-106R7808) to Y.-W.L. and the National Science Foundation (grant NSF-1612917) to A.P.L.

Supplementary information

Supplementary information available online at
http://jcs.biologists.org/lookup/doi/10.1242/jcs.232579.supplemental

References

Akimov, S. A., Kuzmin, P. I., Zimmerberg, J. and Cohen, F. S. (2007). Lateral tension increases the line tension between two domains in a lipid bilayer membrane. *Phys. Rev. E* **75**, 011919. doi:10.1103/PhysRevE.75.011919

Antonescu, C. N., Danuser, G. and Schmid, S. L. (2010). Phosphatidic acid plays a regulatory role in clathrin-mediated endocytosis. *Mol. Biol. Cell* **21**, 2944-2952. doi:10.1091/mbc.e10-05-0421

Antonny, B., Burd, C., De Camilli, P., Chen, E., Daumke, O., Faelber, K., Ford, M., Frolov, V. A., Frost, A., Hinshaw, J. E. et al. (2016). Membrane fission by dynamin: what we know and what we need to know. *EMBO J.* **35**, 2270-2284. doi:10.15252/embj.201694613

Bloomfield, G. and Kay, R. R. (2016). Uses and abuses of macropinocytosis. *J. Cell Sci.* **129**, 2697-2705. doi:10.1242/jcs.176149

Boulant, S., Kural, C., Zeeh, J.-C., Ubelmann, F. and Kirchhausen, T. (2011). Actin dynamics counteract membrane tension during clathrin-mediated endocytosis. *Nat. Cell Biol.* **13**, 1124-1131. doi:10.1038/ncb2307

Brown, H. A., Henage, L. G., Preininger, A. M., Xiang, Y. and Exton, J. H. (2007). Biochemical analysis of phospholipase D. *Methods Enzymol.* **434**, 49-87. doi:10.1016/S0076-6879(07)34004-4

Buckley, C. M. and King, J. S. (2017). Drinking problems: mechanisms of macropinosome formation and maturation. *FEBS J.* **284**, 3778-3790. doi:10.1111/febs.14115

Chen, D. and Santore, M. M. (2014). Large effect of membrane tension on the fluid-solid phase transitions of two-component phosphatidylcholine vesicles. *Proc. Natl. Acad. Sci. USA* **111**, 179-184. doi:10.1073/pnas.1314993111

Clayton, E. L. and Cousin, M. A. (2009). The molecular physiology of activity-dependent bulk endocytosis of synaptic vesicles. *J. Neurochem.* **111**, 901-914. doi:10.1111/j.1471-4159.2009.06384.x

Colley, W. C., Sung, T.-C., Roll, R., Jenco, J., Hammond, S. M., Altshuller, Y., Bar-Sagi, D., Morris, A. J. and Frohman, M. A. (1997). Phospholipase D2, a distinct phospholipase D isoform with novel regulatory properties that provokes cytoskeletal reorganization. *Curr. Biol.* **7**, 191-201. doi:10.1016/S0960-9822(97)70090-3

Conner, S. D. and Schmid, S. L. (2003). Regulated portals of entry into the cell. *Nature* **422**, 37-44. doi:10.1038/nature01451

Dai, J. and Sheetz, M. P. (1995). Regulation of endocytosis, exocytosis, and shape by membrane tension. *Cold Spring Harb. Symp. Quant. Biol.* **60**, 567-571. doi:10.1101/SQB.1995.060.01.060

Diz-Muñoz, A., Fletcher, D. A. and Weiner, O. D. (2013). Use the force: membrane tension as an organizer of cell shape and motility. *Trends Cell Biol.* **23**, 47-53. doi:10.1016/j.tcb.2012.09.006

Diz-Muñoz, A., Thurley, K., Chintamen, S., Altschuler, S. J., Wu, L. F., Fletcher, D. A. and Weiner, O. D. (2016). Membrane tension acts through PLD2 and mTORC2 to limit actin network assembly during neutrophil migration. *PLoS Biol.* **14**, e1002474. doi:10.1371/journal.pbio.1002474

Doherty, G. J. and McMahon, H. T. (2009). Mechanisms of endocytosis. *Annu. Rev. Biochem.* **78**, 857-902. doi:10.1146/annurev.biochem.78.081307.110540

Du, G. W., Huang, P., Liang, B. T. and Frohman, M. A. (2004). Phospholipase D2 localizes to the plasma membrane and regulates angiotensin II receptor endocytosis. *Mol. Biol. Cell* **15**, 1024-1030. doi:10.1091/mbc.e03-09-0673

Gauthier, N. C., Masters, T. A. and Sheetz, M. P. (2012). Mechanical feedback between membrane tension and dynamics. *Trends Cell Biol.* **22**, 527-535. doi:10.1016/j.tcb.2012.07.005

Haga, Y., Miwa, N., Jahangeer, S., Okada, T. and Nakamura, S. (2009). CtBP1/BARS is an activator of phospholipase D1 necessary for agonist-induced macropinocytosis. *EMBO J.* **28**, 1197-1207. doi:10.1038/emboj.2009.78

Hamada, T., Kishimoto, Y., Nagasaki, T. and Takagi, M. (2011). Lateral phase separation in tense membranes. *Soft Mat.* **7**, 9061-9068. doi:10.1039/c1sm05948c

Holst, M. R., Vidal-Quadras, M., Larsson, E., Song, J., Hubert, M., Blomberg, J., Lundborg, M., Landström, M. and Lundmark, R. (2017). Clathrin-independent endocytosis suppresses cancer cell blebbing and invasion. *Cell Rep.* **20**, 1893-1905. doi:10.1016/j.celrep.2017.08.006

Hornberger, T. A., Chu, W. K., Mak, Y. W., Hsiung, J. W., Huang, S. A. and Chien, S. (2006). The role of phospholipase D and phosphatidic acid in the mechanical activation of mTOR signaling in skeletal muscle. *Proc. Natl. Acad. Sci. USA* **103**, 4741-4746. doi:10.1073/pnas.0600678103

Hornberger, T. A., Sukhija, K. B., Wang, X.-R. and Chien, S. (2007). mTOR is the rapamycin-sensitive kinase that confers mechanically-induced phosphorylation of the hydrophobic motif site Thr(389) in p70(S6k). *FEBS Lett.* **581**, 4562-4566. doi:10.1016/j.febslet.2007.08.045

Houk, A. R., Jilkine, A., Mejean, C. O., Boltyanskiy, R., Dufresne, E. R., Angenent, S. B., Altschuler, S. J., Wu, L. F. and Weiner, O. D. (2012). Membrane tension maintains cell polarity by confining signals to the leading edge during neutrophil migration. *Cell* **148**, 175-188. doi:10.1016/j.cell.2011.10.050

Jiang, Y., Sverdlov, M. S., Toth, P. T., Huang, L. S., Du, G. W., Liu, Y. Y., Natarajan, V. and Minshall, R. D. (2016). Phosphatidic acid produced by RalA-activated PLD2 stimulates caveolae-mediated endocytosis and trafficking in endothelial cells. *J. Biol. Chem.* **291**, 20729-20738. doi:10.1074/jbc.M116.752485

Kosmalska, A. J., Casares, L., Elosegui-Artola, A., Thottacherry, J. J., Moreno-Vicente, R., González-Tarragó, V., del Pozo, M. A., Mayor, S., Arroyo, M., Navajas, D. et al. (2015). Physical principles of membrane remodelling during cell mechanoadaptation. *Nat. Commun.* **6**, 7292. doi:10.1038/ncomms8292

Levin, R., Grinstein, S. and Schlam, D. (2015). Phosphoinositides in phagocytosis and macropinocytosis. *Biochim. Biophys. Acta* **1851**, 805-823. doi:10.1016/j.bbalip.2014.09.005

Lin, S.-S. and Liu, Y.-W. (2019). Mechanical stretch induces mTOR recruitment and activation at the phosphatidic acid-enriched macropinosome in muscle cell. *Front. Cell Dev. Biol.* **7**, 78. doi:10.3389/fcell.2019.00078

Liu, A. P. and Fletcher, D. A. (2006). Actin polymerization serves as a membrane domain switch in model lipid bilayers. *Biophys. J.* **91**, 4064-4070. doi:10.1529/biophysj.106.090852

Liu, Y.-W., Surka, M. C., Schroeter, T., Lukiyanchuk, V. and Schmid, S. L. (2008). Isoform and splice-variant specific functions of dynamin-2 revealed by analysis of conditional knock-out cells. *Mol. Biol. Cell* **19**, 5347-5359. doi:10.1091/mbc.e08-08-0890

Liu, Y., Su, Y. and Wang, X. (2013). Phosphatidic acid-mediated signaling. *Adv. Exp. Med. Biol.* **991**, 159-176. doi:10.1007/978-94-007-6331-9_9

Liu, A. P., Botelho, R. J. and Antonescu, C. N. (2017). The big and intricate dreams of little organelles: embracing complexity in the study of membrane traffic. *Traffic* **18**, 567-579. doi:10.1111/tra.12497

Lo, H. P., Nixon, S. J., Hall, T. E., Cowling, B. S., Ferguson, C., Morgan, G. P., Schieber, N. L., Fernandez-Rojo, M. A., Bastiani, M., Floetenmeyer, M. et al. (2015). The caveolin-cavin system plays a conserved and critical role in mechanoprotection of skeletal muscle. *J. Cell Biol.* **210**, 833-849. doi:10.1083/jcb.201501046

Marie-Anaïs, F., Mazzolini, J., Herit, F. and Niedergang, F. (2016). Dynamin-actin cross talk contributes to phagosome formation and closure. *Traffic* **17**, 487-499. doi:10.1111/tra.12386

Masters, T. A., Pontes, B., Viasnoff, V., Li, Y. and Gauthier, N. C. (2013). Plasma membrane tension orchestrates membrane trafficking, cytoskeletal remodeling, and biochemical signaling during phagocytosis. *Proc. Natl. Acad. Sci. USA* **110**, 11875-11880. doi:10.1073/pnas.1301766110

Nassoy, P. and Lamaze, C. (2012). Stressing caveolae new role in cell mechanics. *Trends Cell Biol.* **22**, 381-389. doi:10.1016/j.tcb.2012.04.007

Oglęcka, K., Rangamani, P., Liedberg, B., Kraut, R. S. and Parikh, A. N. (2014). Oscillatory phase separation in giant lipid vesicles induced by transmembrane osmotic differentials. *eLife* **3**, e03695. doi:10.7554/eLife.03695

Petersen, E. N., Chung, H.-W., Nayebosadri, A. and Hansen, S. B. (2016). Kinetic disruption of lipid rafts is a mechanosensor for phospholipase D. *Nat. Commun.* **7**, 13873. doi:10.1038/ncomms13873

Portet, T., Gordon, S. E. and Keller, S. L. (2012). Increasing membrane tension decreases miscibility temperatures; an experimental demonstration via micropipette aspiration. *Biophys. J.* **103**, L35-L37. doi:10.1016/j.bpj.2012.08.061

Saleem, M., Morlot, S., Hohendahl, A., Manzi, J., Lenz, M. and Roux, A. (2015). A balance between membrane elasticity and polymerization energy sets the shape of spherical clathrin coats. *Nat. Commun.* **6**, 6249. doi:10.1038/ncomms7249

Scita, G. and Di Fiore, P. P. (2010). The endocytic matrix. *Nature* **463**, 464-473. doi:10.1038/nature08910

Shi, Z. and Baumgart, T. (2015). Membrane tension and peripheral protein density mediate membrane shape transitions. *Nat. Commun.* **6**, 5974. doi:10.1038/ncomms6974

Sinha, B., Köster, D., Ruez, R., Gonnord, P., Bastiani, M., Abankwa, D., Stan, R. V., Butler-Browne, G., Vedie, B., Johannes, L. et al. (2011). Cells respond to mechanical stress by rapid disassembly of caveolae. *Cell* **144**, 402-413. doi:10.1016/j.cell.2010.12.031

Tan, X., Heureaux, J. and Liu, A. P. (2015). Cell spreading area regulates clathrin-coated pit dynamics on micropatterned substrate. *Integr. Biol.* **7**, 1033-1043. doi:10.1039/C5IB00111K

Teng, S., Stegner, D., Chen, Q., Hongu, T., Hasegawa, H., Chen, L., Kanaho, Y., Nieswandt, B., Frohman, M. A. and Huang, P. (2015). Phospholipase D1 facilitates second-phase myoblast fusion and skeletal muscle regeneration. *Mol. Biol. Cell* **26**, 506-517. doi:10.1091/mbc.E14-03-0802

Thottacherry, J. J., Kosmalska, A. J., Kumar, A., Vishen, A. S., Elosegui-Artola, A., Pradhan, S., Sharma, S., Singh, P. P., Guadamillas, M. C., Chaudhary, N. et al. (2018). Mechanochemical feedback control of dynamin independent endocytosis modulates membrane tension in adherent cells. *Nat. Commun.* **9**, 4217. doi:10.1038/s41467-018-06738-5

Tomassen, S. F. B., van der Wijk, T., de Jonge, H. R. and Tilly, B. C. (2004). Activation of phospholipase D by osmotic cell swelling. *FEBS Lett.* **566**, 287-290. doi:10.1016/j.febslet.2004.04.063

Tsujita, K., Takenawa, T. and Itoh, T. (2015). Feedback regulation between plasma membrane tension and membrane-bending proteins organizes cell polarity during leading edge formation. *Nat. Cell Biol.* **17**, 749-758. doi:10.1038/ncb3162

Ursell, T. S., Klug, W. S. and Phillips, R. (2009). Morphology and interaction between lipid domains. *Proc. Natl. Acad. Sci. USA* **106**, 13301-13306. doi:10.1073/pnas.0903825106

Wang, J. T. H., Teasdale, R. D. and Liebl, D. (2014). Macropinosome quantitation assay. *MethodsX* **1**, 36-41. doi:10.1016/j.mex.2014.05.002

Weinberg, J. and Drubin, D. G. (2012). Clathrin-mediated endocytosis in budding yeast. *Trends Cell Biol.* **22**, 1-13. doi:10.1016/j.tcb.2011.09.001

Wesołowska, O., Michalak, K., Maniewska, J. and Hendrich, A. B. (2009). Giant unilamellar vesicles - a perfect tool to visualize phase separation and lipid rafts in model systems. *Acta Biochim. Pol.* **56**, 33-39. doi:10.18388/abp.2009_2514

Xie, Z., Ho, W.-T. and Exton, J. H. (2002). Functional implications of post-translational modifications of phospholipases D1 and D2. *Biochim. Biophys. Acta* **1580**, 9-21. doi:10.1016/S1388-1981(01)00168-8

Yang, C.-Y. and Frohman, M. A. (2012). Mitochondria: signaling with phosphatidic acid. *Int. J. Biochem. Cell Biol.* **44**, 1346-1350. doi:10.1016/j.biocel.2012.05.006

Yarar, D., Waterman-Storer, C. M. and Schmid, S. L. (2007). SNX9 couples actin assembly to Phosphoinositide signals and is required for membrane remodeling during endocytosis. *Dev. Cell* **13**, 43-56. doi:10.1016/j.devcel.2007.04.014

Yoshida, S., Pacitto, R., Inoki, K. and Swanson, J. (2018). Macropinocytosis, mTORC1 and cellular growth control. *Cell. Mol. Life Sci.* **75**, 1227-1239. doi:10.1007/s00018-017-2710-y

Zeniou-Meyer, M., Zabari, N., Ashery, U., Chasserot-Golaz, S., Haeberlé, A.-M., Demais, V., Bailly, Y., Gottfried, I., Nakanishi, H., Neiman, A. M. et al. (2007). Phospholipase D1 production of phosphatidic acid at the plasma membrane promotes exocytosis of large dense-core granules at a late stage. *J. Biol. Chem.* **282**, 21746-21757. doi:10.1074/jbc.M702968200